Electrochemical characterization of flat-plate rechargeable alkaline manganese dioxide–zinc cells

P.R. Roberge and M. Farahani
Department of Chemistry & Chemical Engineering, Royal Military College of Canada, Kingston, Ont., K7K 5L0 (Canada)

K. Tomantschger and E. Oran
Battery Technologies Inc., 30 Pollard Street, Richmond Hill, Ont., L4B 1C3 (Canada)

(Received and accepted May 12, 1993)

Abstract

The electrochemical characterization of flat-plate rechargeable alkaline manganese/dioxide–zinc (RAM) cells was made with various techniques throughout their cycle life. The two chemistries evaluated in this study behave quite differently throughout their cycle life. While the chemistry commonly used in cylindrical cells provided an excellent first cycle, its capacity diminished quite rapidly during the following cycles. The cells containing a $Ca(OH)_2$ anode additive, on the other hand, delivered rather poor initial cycles but their performance improved towards the third cycle and remained at that level throughout a much longer practical cycle life. Electrochemical impedance spectroscopy measurements performed at regular intervals of the cycle life of the flat-plate cells indicated that the overall impedance of cells containing a $Ca(OH)_2$ additive was controlled by charge-transfer processes at the negative electrode. Electrochemical noise measurements were also carried out at regular intervals with very sensitive equipment and the results obtained permitted to confirm that the electrochemical noise generated by the flat-plate cells can be completely explained by stochastic processes.

Introduction

Rechargeable alkaline manganese dioxide–zinc (RAM) technology

The first 'dry cells' of the alkaline MnO_2–Zn type were probably those developed by Achenbach and which used zinc wire fabric anodes imbedded in gelled KOH or NaOH electrolytes [1, 2]. During the following years the alkaline cell technology efforts were concentrated on the development of CuO cells and air-depolarized (wet) cells. It is only after HgO cells had been successfully developed under the World War II pressure that the development of an alkaline MnO_2 cell was considered again. The development work of Herbert [3] in the mid 1950s led to the production of the 'Crown' cells which had low drain and were particularly used in 9 V radio batteries. It was then a common belief that the MnO_2–Zn system was only capable of low current outputs. This situation changed considerably when further developments revealed that the MnO_2–Zn system could deliver far higher currents and provide more capacity at heavy loads than the Leclanché system itself. The conventional bobbin-can arrangement was abandoned during this development and the outside sleeve cathode coupled with powder zinc anode were introduced. Most of this work was carried out at the Union Carbide Corp. Laboratories [4].

The rechargeability of the alkaline MnO_2–Zn system was recognized as early as 1950 [5] and the first commercial products appeared on the market in the late sixties. These early cells, which were modified primary cells utilizing inorganic binders in the cathode and improved separators, required customer attention or electronic means to detect the end of discharge [6, 7]. The production of this early technology ceased mostly due to the inability of the cells to withstand any consumer abuse. Anode limitation was suggested as method to overcome these problems as early as 1970 [8]. In this design the theoretical capacity of the zinc electrode was reduced to between 20 to 30% of the theoretical one electron MnO_2 capacity by replacing some of the zinc gel with gelled electrolyte. The resulting cells could withstand consumer abuse such as overdischarge but suffered from low-energy content and poor high-rate performance.

In 1987 Battery Technologies Inc. (BTI) commenced the commercial development of the RAM technology and in 1989 a production facility was established for cylindrical AA RAM cells. The BTI cells are based on the anode limitation technique but with an improved internal design which resulted in optimization of the active-material utilization and thus an increased energy density.

In the cylindrical cell consumer market, RAM cells have become an economically and viable alternative to single use zinc–carbon and alkaline batteries. Most cell components and raw materials used are identical to those used in primary alkaline cells. The major design changes made to primary alkaline cells lie in cathode and anode formulations, the limitation of the anode capacity to less than the first electron capacity of the MnO_2 cathode, the addition of barrier layers to the separator and the integration of means to enable moderate cell abuse [9, 10]. Depending on the operating conditions, between 7 to 20 times the operating time of primary alkaline cells and 35 to 100 times that of zinc–carbon cells has been achieved in low-mercury and mercury-free cell designs. Current AA RAM cells deliver, during their first cycle, in excess of 125% of the International Electrotechnical Commission (IEC) minimum average for primary alkaline cells and in excess of 80% of the performance of the leading primary alkaline cells on the market. The manufacturing cost of RAM cells is within 120% of the cost of alkaline throwaway cells and the mercury content of commercial design RAM cells has been reduced to the level of present alkaline cells (0.025% of cell weight).

The flat-plate electrode design is the next logical step to extend the capabilities of the MnO_2–Zn system to larger applications. It was found that the flat-plate arrangement gave the RAM technology very high current-carrying capabilities which could rival commercially available Ni–Cd batteries while keeping reasonably good rechargeability. The low cost and availability of raw materials going into the fabrication of the RAM cells were of course retained. It has been reported that the charge retention of the RAM system was found to be far superior to either Ni–Cd or Ag–Zn rechargeables, especially at elevated temperatures where these other technologies lose their capacity rapidly [11]. In fact, the self-discharge behavior of the RAM cells in their cylindrical or flat-plate versions was found to be comparable with the well-characterized cylindrical MnO_2–Zn alkaline primaries [11]. The energy density, on the other hand, can be as high as twice that of a lead/acid cell and the presence of the KOH electrolyte keeps this high performance characteristic to very low temperatures [11].

Flat-plate technology

To assure the integrity of the MnO_2 flat-plate cathodes, a plastic bonding was judged to be essential. It was determined that, without a binder, flat-plate cathodes

would simply disintegrate when subjected to the phase changes which occur during cycling. This approach stands in contrast with the fabrication of cathodes used in cylindrical cells where the steel container serves to restrict expansion and keep the cathodic material intact [9].

Plastic bonding is known as a practical method to produce thin battery plates. The effect of the plastic bonding depends on the discharge mechanisms involved at each electrode. For battery-discharge reactions where only one solid phase transformation occurs, plastic bonding is quite effective since the physical structure of the active material remains essentially unchanged. This is the case of the active MnO_2 material for which the particles would only change by 10 to 15% during a complete cycle. Thin plate electrodes bear several advantages over thick 'sleeve' electrodes such as: (i) excellent high rate capability; (ii) good rechargeability, and (iii) increased active material utilization, particularly at high rate.

A significant number of studies have been made on secondary zinc electrodes used in alkaline electrolytes. Most of this work has focused on zinc electrodes for zinc–nickel oxide battery systems [12, 13]. Such zinc electrodes are normally assembled in the discharged state using ZnO. Furthermore, the nickel oxide electrode is the capacity-limiting electrode and a high stoichiometric Zn:Ni ratio, typically 3:1, is maintained [12]. In order to suppress the shape change of the zinc electrode, sufficient $Ca(OH)_2$ is added to insure the precipitation of all zinc discharge products as calcium zincate [12–15] and no excess electrolyte is provided (starved electrolyte cells). The concentration of KOH in these cells is lowered down to typically 1.9 M (10%) to further improve the cycle life [12, 16]. Other electrolyte additives, such as borates or a combination of boric acid, phosphoric acid and arsenic acid are also used [17] to improve the cycle life of these cells.

Secondary zinc electrodes used in manganese dioxide–zinc or zinc/air cells are normally assembled in the fully-charged state and the metallic zinc electrodes are capacity limiting. Only a limited amount of information is available in the published literature on these zinc electrodes. Such zinc electrodes not using a $Ca(OH)_2$ additive have been reported to provide between 30 and 50 deep-discharge cycles in a starved electrolyte zinc–zinc cell arrangement with 80% initial and 50% end-of-life capacity utilization [18]. No information exists for cells containing a MnO_2-positive electrode which is known to irreversibly precipitate zincate in the form of haeterolite ($Mn_2O_3 \cdot ZnO$).

Consequently, a study investigating the performance of secondary zinc electrodes with and without means to reduce the solubility of discharged zinc species in zinc-limited MnO_2–zinc cells was to provide valuable information for the development of flat-plate MnO_2–Zn cells. Since the rate capability of MnO_2–Zn cells was found to suffer significantly, when the electrolyte concentration was low, a 9 M (37%) KOH solution was used throughout the present study. One set of cells was made with zinc electrodes without means to reduce the zincate solubility whereas another set contained a $Ca(OH)_2$ additive. To accelerate the effects produced by the interaction of the various zinc species and the MnO_2 electrode, all cells contained an excess of electrolyte (flooded cells).

Electrochemical testing

The electrochemical characterization of the cells was made with various techniques throughout their cycle life. The internal resistance at 1 kHz and electrochemical impedance spectroscopy (EIS) measurements were made at regular intervals during the lifetime of the cells tested. By carrying out impedance measurements with a three-electrode configuration it was possible to develop individual electrode models constructed

of the impedance main components, i.e., the charge-transfer resistance (R_{ct}) in parallel to the double-layer capacitance (C_{dl}). A third parameter calculated from the EIS data expresses the angle of tilt that is a common feature of EIS Nyquist plots and is apparent in the capacitive range of log(Z) versus log(f) Bode diagrams [19] as a digression from slope (β) value unity. The empirical factor which has to be introduced into the mathematical procedures to fit EIS data would appear as an exponent α with a value between 0 and 1, which would be added to the imaginary component of an impedance frequency (ω) response $Z(\omega)$ (eqn. 1):

$$Z(\omega) = R_s + \frac{R_{ct}}{1 + (j\omega R_{ct} C_{dl})^{\beta}} \quad (1)$$

The constant phase element (CPE) corresponding to this empirical factor has often been associated with dispersion effects [20–22] that, in the present case, could be due to a multitude of factors related to the series of interfaces involved between the positive and negative electrodes. The presence and magnitude of the CPE has been demonstrated to be of practical significance for monitoring the health and reliability [23–25] of some chemical power sources (Li/SO_2) that can be modeled with relatively simple equivalent circuits.

The voltage fluctuations of the baseline discharge voltage were also recorded during discharge at different moments of the cells' cycle life. These voltage fluctuations were analyzed with a novel analysis technique which relies on the stochastic nature of the voltage fluctuations [26] to transform the information visibly present in the recorded noise spectra into quantitative variables.

The study of chemical oscillations and electrochemical fluctuations has always fascinated scientists but most of the electrochemical noise work published to date has focused on phenomena associated with corrosion studies. Only a few papers have been published [26–32] reporting studies of voltage fluctuations in association with the operation of battery systems. The usefulness of monitoring voltage noise patterns observed during the various phases of charging sealed lead/acid cells was demonstrated [31] by associating the origin of noise signals to problems associated with either the operation of the positive electrode during the earlier phases of charging the cells or the behavior of the negative electrode towards the end of charging. It was also demonstrated that the baseline noise recorded during the simple resistive discharge of Li/SO_2 and $LiSOCl_2$ cells [32] was related to fundamental characteristics such as cell type and depth-of-discharge and, more recently, that the same technique could be used to highlight some salient features of the RAM technology itself [26].

Experimental

Two types of cells were fabricated for the present study. One type used the same chemistry normally adopted to fabricate cylindrical cells and the other contained a solid $Ca(OH)_2$ additive mixed with the anode to reduce the solubility of secondary zinc electrode discharge products. The addition of stoichiometric quantities of $Ca(OH)_2$ to the zinc electrode, in conjunction with the use of a concentrated electrolyte (9 N KOH) and microporous noncellulosic separators, have frequently been used in cells with limited solubility zinc electrodes [12, 13].

The fabrication techniques employed for the construction of the flat-plate RAM cells were similar to those commonly practiced during the fabrication of lead/acid battery electrodes. The active materials were prepared in the form of relatively stiff

pastes by mixing homogenized solid compounds with a mixture of binder and water and applying the pastes thus formed to the current collector grids by a combination of pasting, rolling and pressing steps. A silver mesh was used as the current collector for the MnO_2 electrode. The zinc electrodes were prepared by applying the paste to a tin-plated copper screen. These zinc electrodes did not contain mercury but hydrogen gassing was suppressed by the addition of a combination of organic and inorganic inhibitors. Polytetrafluoroethylene (PTFE) was used as the binder for the preparation of all electrodes and no organic solvents were used for the fabrication of these cells.

Electrodes were fabricated using pasting, pressing and curing operations. Multi-component envelope-type separators were used for both the MnO_2 and the zinc electrodes. The separators extended past the electrodes and were folded back onto themselves thereby not requiring the need of heat sealing. Each cell was assembled by sandwiching one 50 cm^2 active area zinc electrode, with a 9 Ah theoretical zinc capacity, between two MnO_2 electrodes. The cells were finally activated by inserting an excess of 9 N KOH electrolyte. The leads of the two electrodes were fed through the casing to the outside and a small aperture located above the top of the separator permitted to introduce a reference electrode (a freshly-polished strip of Zn metal) which would come into electrolytic contact with the cell. Figure 1 shows a schematic description of a single-cell flat-plate assembly used in this study.

The internal resistance (R_{ir}) of fully-charged cells was measured with a commercial milliohmmeter (HP Model 4328A) and EIS measurements were obtained with a commercial frequency response analyzer (FRA) (Solartron Model 1253) equipped with a potentiostat/galvanostat (Solartron Model 1186).

The voltage fluctuations were monitored between three points of the flat-plate cells, the anode collector, the cathode collector and a zinc reference electrode during purely resistive (1.5 Ω) deep discharge. The voltage fluctuations between the reference electrode and the anode material were recorded directly while a high-pass filter was used for the other two configurations (between the positive material and the reference electrode or between the anode and cathode). The filter consisted of a 1 MΩ resistor in parallel with a 1 μF capacitor for a lower frequency cutoff (f_c) at 0.16 Hz. Its utilization permitted to increase the sensitivity of the measurement technique (30 mV scale of the HP 3457A multimeter gives a resolution of 10 nV).

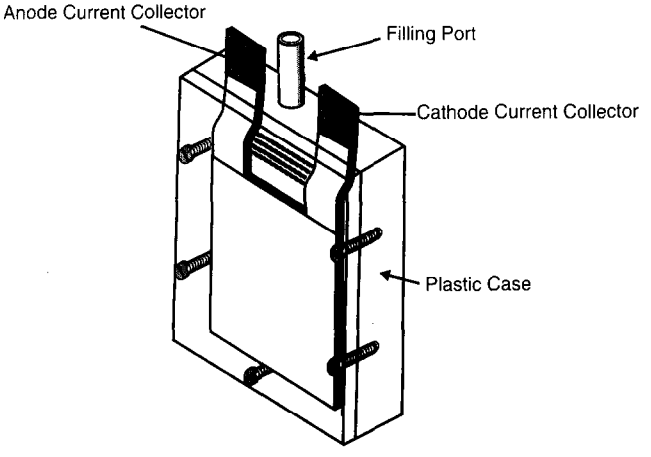

Fig. 1. Schematic description of a single RAM flat-cell assembly construction.

A sampling interval (Δt) of 0.3 s and a number of consecutive data points (N) of 4000 were chosen since they allowed access to the frequency domain where electrochemical processes are dominant [33, 34]. The frequency domain corresponding to these sampling conditions can be evaluated to be between 1.67 Hz (f_{max}) and 0.8 mHz (f_{min}) with the help of eqns. (2) and (3) [35]. But since the use of a high-pass filter in these studies will have affected the shapes and amplitudes of the voltage fluctuations differently depending on their relation with the f_c (unaffected above f_c and as dV/dt under f_c) the information extracted from the lower frequency domain, when a filter was used, can only be used in a relative fashion:

$$f_{max} = \frac{1}{2\Delta t} \tag{2}$$

$$f_{min} = \frac{1}{N\Delta t} \tag{3}$$

Results and discussion

Routine performance evaluation included the internal resistance measurement at 1 kHz, open-circuit (OCV) and closed-circuit (CCV) voltage measurements followed by shallow- and deep-discharge cycling tests. A set of two identical cells was used for each cycling test. Occasionally polarization curves were obtained and each electrode potential was determined against the reference electrode. The shallow-discharge test consisted of discharging the cells using a 6 Ω load resistor ($\approx$200 mA) for 4 h per day and 7 days per week. Cells containing the calcium additive were cycled on this regime for 1 week before being put to the deep-discharge tests. Some cells tested solely with the shallow-testing profile gave 275 cycles before cell failure occurrence.

During the deep-cycle test, cells were discharged using a 2.2 Ω load resistor (approximately 550 mA average current) to 0.9 V and then recharged within 24 h. The rechargeability of a given cell being cycled will depend on a variety of parameters. For the present purpose the rechargeability was defined as the number of cycles a cell would deliver until it reached a practical cutoff capacity of 1.5 Ah. Figure 2 illustrates the capacity values obtained when the two chemistries evaluated in the present study were deep discharged through their cycle life. It can be observed that the two systems behave quite differently. While the cylindrical chemistry provided an excellent first cycle, the capacity values obtained during the following cycles were drastically reduced. This degradation was attributed to the formation of haeterolite. The charge capacity provided during the first recharge was determined to be merely a fraction (30%) of the initial discharge capacity. This drastic loss (70%) of capacity observed for the flat-plate cells had not been observed for cylindrical RAM cells of identical chemistry where the capacity drop after the initial charge rarely exceeded 20% [36]. This difference in behavior was attributed to the difference in electrode thickness of both electrodes between the 'bobbin type' electrodes and the thin electrode flat-plate cells and to the difference in electrolyte management between the 'starved' cylindrical and 'flooded' flat-plate cells. The excess electrolyte present in the flat-plate cells in combination with thinner electrodes would increase the relative mobility of zincate ions within these cells to the detriment of their performance. But one could still get quite a few practical cycles out of such cells ($\approx$25 cycles in Fig. 2).

The cells containing the $Ca(OH)_2$ anode additive, on the other hand, delivered rather poor initial cycles but their performance improved towards the third cycle and

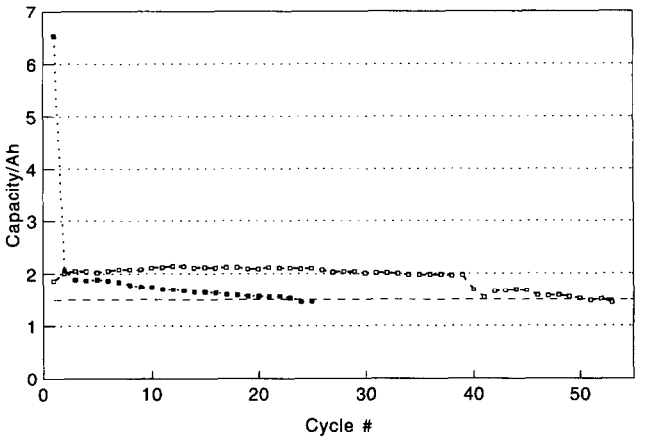

Fig. 2. Deep cycling performance obtained with the two flat-plate RAM technologies tested during this study: (□) with $Ca(OH)_2$ additive, and (■) cylindrical cell chemistry.

remained at that level throughout a much longer practical cycle life ($\approx$55 cycles in Fig. 2). The poor utilization of the zinc-active material ($\approx$22%) in these cells was attributed to low electrode porosity which provided a limiting access by the electrolyte.

EIS results

The analyzed EIS results obtained at every 10 cycles during the cycle life of flat-plate RAM cells are presented in Table 1 (cylindrical cell chemistry) and Table 2 ($Ca(OH)_2$ additive). The measured and calculated parameters presented in Tables 1 and 2 do not reflect the complete reality of the EIS responses gathered at various moments of charge and cycle life of the two cells tested in this study. The simple fact that the measurements were made on large (50 cm^2) and porous or rough surfaces is normally associated with diffused EIS patterns. The high values of CPE calculated for most of these EIS measurements indicate clearly the high degree of dispersion one can observe when working with such complex surfaces. But some striking features can nonetheless be remarked by analyzing the EIS data. One, for example, can observe the stability of the internal resistance measurements (R_{ir}) which seem to be completely independent of the cycle life, the charge state in each cycle or even the cell chemistry [29 mΩ average in both cases).

Another feature was highlighted by adding, in these Tables, the individual charge resistance (R_{ct}) values calculated for each electrode and comparing these sums with the results which had been obtained for the complete cell measurements. It can be seen that these sums agree relatively well with the complete cell measurements. This would confirm that even the crude models which were assumed for the study of these complex interfaces can give a good indication concerning the fundamental impedance characteristics controlling the electrochemical reactions. The presence of diffusional constraints (Fig. 3), which are clearly visible (slope $\log(Z)/\log(f) \approx 0.5$) in the low-frequency portion of the Bode plots of EIS results obtained from the positive electrode, would indicate that the operation of the positive electrode is controlled by mass-transport limitations. But the main contribution to the impedance of these cells seems to be imposed, as designed, by charge-transfer processes at the negative electrode (Fig. 4) which are closer in value and shape to the global cells' low-frequency EIS measurements (Fig. 5).

TABLE 1

Analyzed EIS results obtained during the cycle life of a flat-plate RAM cell with a cylindrical cell chemistry

Cycle/ time[a]	R_{ir} (mΩ)	R_{ct} (Ω cm^2)				C_{dl} (mF/cm^2)			τ^e (ms)		β		
		np[b]	n[c]	p[d]	n+p	np	n	p	n	p	np	n	p
10/1	29	20	15	8.0	23	0.82	1.7	0.50	26	4.0	0.59	0.72	0.57
10/2	30	32	13	16	29	0.59	1.0	1.1	13	18	0.63	0.72	0.66
10/3	31	32	5.5	25	31	0.66	0.77	1.0	4.2	25	0.65	0.79	0.62
10/4	31	31	5.2	27	32	0.54	0.66	1.2	3.4	32	0.61	0.8	0.65
20/1	27	29	16	18	34	0.82	2.2	1.4	35	25	0.69	0.65	0.66
20/2	27	24	8.0	14	22	0.81	2.1	1.2	17	17	0.61	0.62	0.71
20/3	27	19	7.7	8.7	16	0.96	2.4	1.9	18	16	0.62	0.43	0.8
20/4	27	17	6.4	7.3	14	1.00	0.77	2.5	4.9	18	0.64	0.53	0.89
μ[f]	29	26	10	16	25	0.8	1.5	1.4	15	19	0.63	0.66	0.70

[a]Time in the discharge (1 = full charge, 2 = 1/3 discharged, 3 = 2/3 discharged, 4 = discharged).
[b]Between negative and positive.
[c]Between negative and reference.
[d]Between positive and reference.
[e]Time constant ($R_{ct}C_{dl}$).
[f]Average values.

Electrochemical noise results

The voltage fluctuations around baseline voltage discharge were analyzed with a new mathematical procedure particularly suitable for the study of stochastic processes. This method, which has been described elsewhere in detail [26, 37], comprised two levels of transformation of the original recordings. At the first level, the voltage fluctuations were transformed into individual positive and negative voltage peaks as basic events. Each directional change of the slope of the recorded voltage served as a trigger to sort and compile the resulting inter-event times (peak duration) in parallel with the rise time of the voltage fluctuations themselves. The rise-time (dV/dt) is considered to be an important characteristic of the electrochemical processes simultaneously occurring at a metallic surface.

The second level of transformation of this noise analysis technique was imported from the field of statistics of event series such as practiced in reliability engineering. Situations in which discrete events occur randomly in a continuum (e.g., time) and which are called stochastic point processes can normally be described by a Poisson probability distribution. For situations where the hazard rate is constant, the Poisson probability distribution can be reduced to an exponential distribution where the characteristic parameter (λ) can be easily obtained by integrating the occurrence distribution of the phenomena that have occurred in a given sample. The characteristic parameter λ was evaluated at a point of the cumulative distribution which corresponds to a computerized version of the classical method to find λ by plotting data on exponential distribution probability papers. The goodness-of-fit of each noise data file was then evaluated by comparing the exponential distributions calculated using the global parameter λ with the experimental distributions observed.

TABLE 2

Analyzed EIS results obtained during the cycle life of a flat-plate RAM cell containing a $Ca(OH)_2$ additive

Cycle/ time[a]	R_{ir} (mΩ)	R_{ct} (Ω cm^2)				C_{dl} (mF/cm^2)			τ^e (ms)		β		
		np[b]	n[c]	p[d]	n+p	np	n	p	n	p	np	n	p
10/1	31	5.9	3.6	3.3	6.9	0.39	0.39	5.8	1.4	19	0.52	0.69	0.85
10/2	29	13	10.1	3.9	14	0.67	0.55	0.92	5.6	3.6	0.5	0.59	0.92
10/3	30	10	5.8	5.4	11	0.18	0.48	0.26	2.8	1.4	0.49	0.64	0.88
10/4	29	11	6.5	5.5	12	0.29	0.52	0.35	3.4	1.9	0.5	0.61	0.82
20/1	27	11	2.8	7.1	10	1.0	1.4	1.2	3.9	8.5	0.54	0.67	0.74
20/2	27	17	13	6.5	20	0.76	1.2	0.82	16	5.3	0.61	0.69	0.68
20/3	28	17	13	6.2	19	0.71	0.60	0.65	7.8	4.0	0.56	0.66	0.68
20/4	27	12	7.2	4.8	12	0.62	0.57	0.45	4.1	2.2	0.48	0.66	0.76
30/1	31	62	61	17	78	0.59	0.96	0.73	59	12	0.68	0.71	0.57
30/2	30	68	56	15	71	0.56	1.1	0.93	62	14	0.61	0.73	0.52
30/3	29	38	21	14	35	0.43	0.76	0.39	16	5.5	0.57	0.69	0.59
30/4	31	19	15	6.4	21	0.66	1.1	0.87	17	5.6	0.54	0.63	0.59
μ[f]	29	24	18	8.0	26	0.6	0.8	1.1	16	7.0	0.55	0.66	0.72

[a]Time in discharge (1 = full charge, 2 = 1/3 discharged, 3 = 2/3 discharged, 4 = discharged).
[b]Between negative and positive.
[c]Between negative and reference.
[d]Between positive and reference.
[e]Time constant ($R_{ct}C_{dl}$).
[f]Average values.

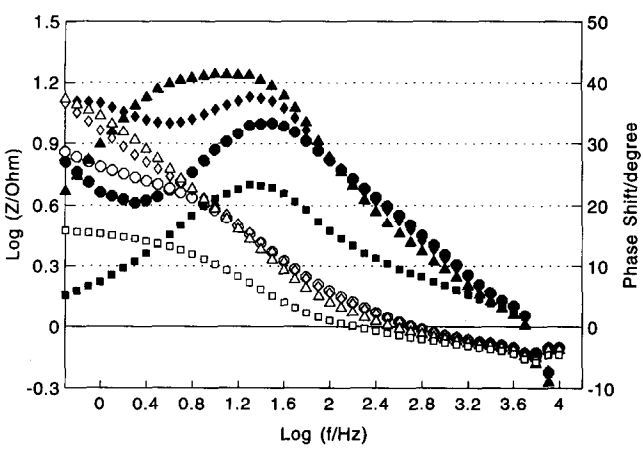

Fig. 3. Bode plots (white symbols) (log(Z) vs. log(f)) and (black symbols) phase shift vs. log(f) of EIS data obtained between the positive plate and a zinc reference electrode of a flat-plate RAM cell containing a $Ca(OH)_2$ additive at cycle 20 and various discharge times; (□) full charge, (△) 1/3 discharged, (◇) 2/3 discharged, and (○) completely discharged.

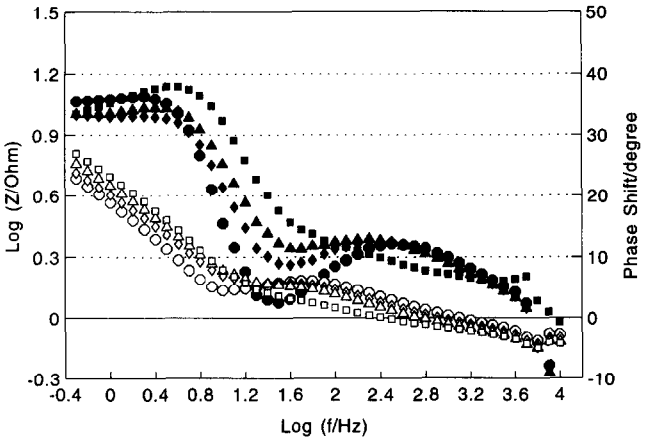

Fig. 4. Bode plots (white symbols) (log(Z) vs. log(f)) and (black symbols) phase shift vs. log(f) of EIS data obtained between the negative plate and a zinc reference electrode of a flat-plate RAM cell containing a $Ca(OH)_2$ additive at cycle 20 and various discharge times; (□) full charge, (△) 1/3 discharged, (◇) 2/3 discharged, and (○) completely discharged.

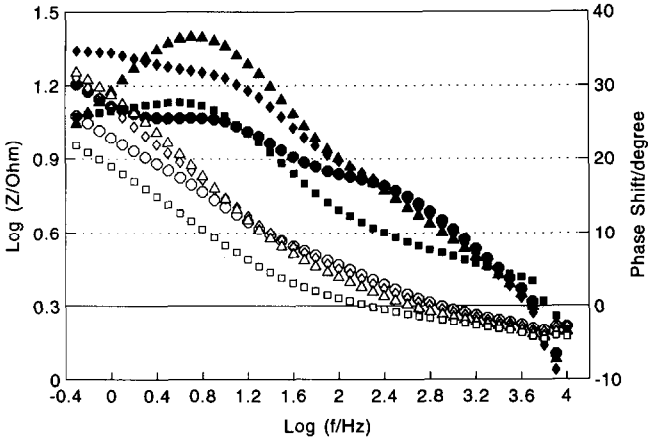

Fig. 5. Bode plots (white symbols) (log(Z) vs. log(f)) and (black symbols) phase shift vs. log(f) of EIS data obtained on a full cell flat-plate RAM cell containing a $Ca(OH)_2$ additive at cycle 20 and various discharge times; (□) full charge, (△) 1/3 discharged, (◇) 2/3 discharged, and (○) completely discharged.

The results obtained by analyzing all the noise files gathered during these experiments are summarized in Table 3 (cylindrical cell chemistry) and Table 4 ($Ca(OH)_2$ additive). The average goodness-of-fit calculated for all the noise records gathered during this study was 99.0%. This is indeed a strong indication that the processes occurring during the discharge of these flat-plate cells are stochastic. While these measurements were made at various discharge times of each cycle reported in these Tables, only the averages are reported since the parameters calculated did not vary appreciably as a function of the relative discharge times. This finding is similar to what had been observed previously [26] with cylindrical RAM cells possessing an extra can coating

TABLE 3

Analyzed electrochemical noise results obtained during the cycle life of a flat-plate RAM cell with a cylindrical cell chemistry

Cycle	1/λ (s)			Rise-time (μV/s)		
	np[a]	n[b]	p[c]	np	n	p
6	0.41	0.39	0.27	4.5	6.3	1.25
12	0.44	0.44	0.32	5.7	7.6	1.4
18	0.48	0.46	0.29	8.8	5.2	1.25
24	0.44	0.45	0.50	134	56	73

[a]Between negative and positive.
[b]Between negative and reference.
[c]Between positive and reference.

TABLE 4

Analyzed electrochemical noise results obtained during the cycle life of a flat-plate RAM cell containing a $Ca(OH)_2$ additive

Cycle	1/λ (s)			Rise-time (μV/s)		
	np[a]	n[b]	p[c]	np	n	p
6	0.60	0.53	0.27	6.4	4.2	1.4
12	0.41	0.39	0.32	7.1	4.0	1.4
18	0.42	0.45	0.30	4.3	3.9	1.2
24	0.48	0.47	0.45	4.2	4.8	4.7
30	0.43	0.46	0.44	4.4	5.2	6.4
36	0.42	0.41	0.40	4.3	4.5	3.9
42	0.44	0.43	0.47	6.0	4.8	6.9
48	0.45	0.42	0.48	116	34	82

[a]Between negative and positive.
[b]Between negative and reference.
[c]Between positive and reference.

added to improve the contact between the active-positive material and the can collector of these cells.

An interesting point to note in Tables 3 and 4 is the constancy of 1/λ and voltage rise-time values over the lifetime of the flat-plate cells tested. The only exceptions can be found near the end of cycle life (cycle 24 of the RAM cell with cylindrical cell chemistry and cycle 48 for the cell containing a $Ca(OH)_2$ additive) when the noise level became exceptionally important and after cycle 24 of the cell containing a $Ca(OH)_2$ additive when the noise signatures between the positive and the reference electrodes became similar to the signatures recorded for the other two configurations. This last transition is illustrated by the noise signatures recorded for three positions during the deep discharge of the flat-plate cell containing a $Ca(OH)_2$ additive at cycle 18

(Fig. 6) and at cycle 24 (Fig. 7). In order to appreciate the degree of quietness observed for these measurements, the voltage fluctuations can be translated in terms relative to the source of the electrochemical noise, i.e., subtle variations of the ohmic resistance of the cells being discharged under a purely resistive load. Using eqn. (4) [37] and approximate values for R_L (1.5 Ω), V (1.0 V) and R_{cell} (30 mΩ) it can be estimated

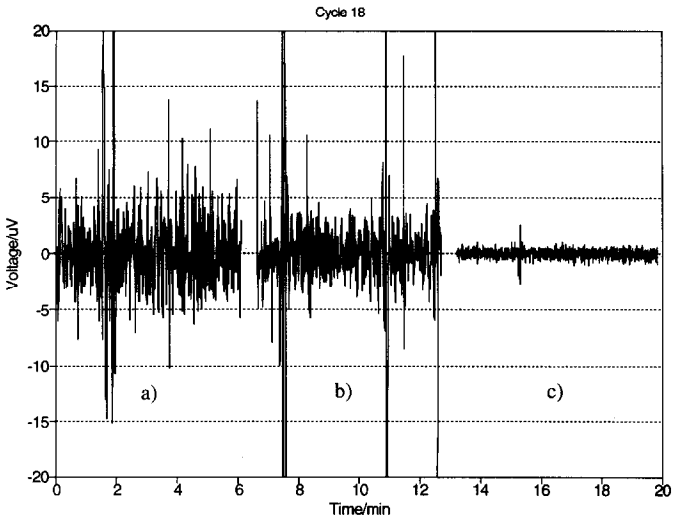

Fig. 6. Voltage fluctuations recorded at cycle 18 of the resistive 1.5 Ω) deep discharge of a flat-plate RAM cell containing a $Ca(OH)_2$ additive: (a) at the cell posts, (b) between a zinc reference and the negative electrode, and (c) between a zinc reference and the positive electrode.

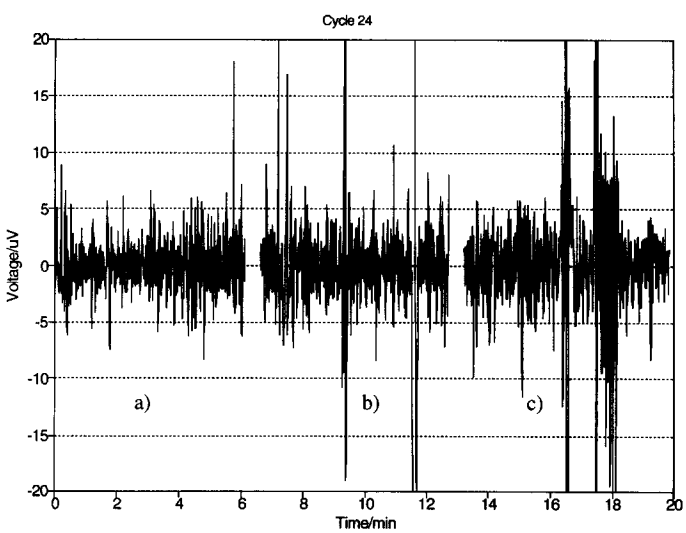

Fig. 7. Voltage fluctuations recorded at cycle 24 of the resistive (1.5 Ω) deep discharge of a flat-plate RAM cell containing a $Ca(OH)_2$ additive: (a) at the cell posts, (b) between a zinc reference and the negative electrode, and (c) between a zinc reference and the positive electrode.

that 5 μV voltage fluctuations in Figs. 5 and 6 would be caused by fluctuations of R_{cell} of approximately 0.025% R_{cell}:

$$\frac{dR_{cell}}{R_{cell}} = -\frac{R_L + R_{cell}}{R_{cell}} \frac{dV}{V} \quad (4)$$

Conclusions

The electrochemical characterization of flat-plate rechargeable alkaline manganese dioxide–zinc (RAM) cells was made with various techniques throughout their cycle life. The two chemistries evaluated in this study behave quite differently throughout their cycle life. While the chemistry commonly used in cylindrical cells provided an excellent first cycle, its capacity dropped drastically after the initial discharge due to the formation of haeterolite. The cells containing a $Ca(OH)_2$ anode additive, on the other hand, delivered rather poor initial cycles but their performance improved in the early cycles and remained at that level throughout a much longer practical cycle life. The EIS results indicated that the internal resistance remained fairly invariant during the discharge of the flat-plate cells and during their cycle life. A good agreement was found between the measured total cell impedance and the impedance calculated with the measured individual electrode impedances demonstrating the validity of the simple model used to analyze the EIS data. The EIS results also indicated that the positive electrode is controlled by mass-transport limitations while the negative electrode, which is overall cell limiting, is itself limited by charge-transfer processes.

The analysis of the electrochemical noise results for their stochastic behavior has been shown in almost perfect fit of all noise records with the predicted decay of peak-population/peak-duration distributions. Such a behavior is strongly indicative that the discharge processes are purely stochastic with no apparent deterministic features. The extremely low level of the electrochemical noise observed during this study and which remained until the end of the cycle life of both cells is another indication that no special process is occurring during the operation of these cells.

This study has shown that the solubility of zincate ions in thin flat-plate RAM cells needs to be suppressed to prevent irreversible capacity loss by formation of haeterolite. This capacity loss, which is exacerbated by the excess of free electrolyte and thin electrode arrangement, can be stabilized by the addition of $Ca(OH)_2$ even in the concentrated KOH electrolyte used in this study. The design, porosity and composition of zinc electrode used in anode-limiting RAM cells need to be further improved to increase the level of active-material utilization in such cells.

References

1 E. Achenbach, *US Patent No. 1 090 372* (1914).
2 E. Achenbach, *US Patent No. 1 098 606* (1914).
3 W.S. Herbert, *J. Electrochem. Soc., 99* (1952) 190C.
4 K.V. Kordesch, Alkaline manganese dioxide batteries, *UCC CRM-285,* Union Carbide Corp., USA, 1973.
5 H.Y. Kang and C.C. Liang, *Electrochim. Acta, 13* (1968) 277.
6 S.U. Falk, *Batteries – Manganese Dioxide,* Vol. 1, Wiley–Interscience, New York, 1969.
7 D. Linden, *Handbook of Batteries and Fuel Cells,* McGraw-Hill, New York, 1984.
8 Y. Amano, *US Patent No. 3 530 496* (1970).

9 K. Tomantschger and C. Michalowski, *US Patent No. 5 108 852* (1992).
10 K. Tomantschger, E. Oran and K.V. Kordesch, *US Patent No. 5 162 169* (1992).
11 K.V. Kordesch, Plastic bonded cathodes for MnO_2–Zn cells, *UCC CRM-300,* Union Carbide Corp., USA, 1973.
12 F. McLarnon and E. Cairns, *J. Electrochem. Soc., 138* (1991) 645.
13 W.V. Van der Grinten, *Ger. Patent No. 1 916 200* (Oct. 23, 1969).
14 G. Krucerca, H.Q. Plust and C. Scheineider, *Society Automotive Engineers, Trans. Paper. No. 750 147,* 1975.
15 R. Jain, T. Adler, F. McLarnon and E. Cairns, *J. Appl. Electrochem., 22* (1992) 1039.
16 E.G. Gagnon, *J. Electrochem. Soc., 138* (1991) 3173.
17 M. Eisenberg, *US Patent No. 4 224 391* (1980).
18 L. Binder, W. Odar and K. Kordesch, *J. Power Sources, 6* (1981) 271.
19 S. Lin, S. Kim, H. Shih and F. Mansfeld, *Electrochim. Acta, 34* (1989) 1123.
20 K.S. Cole and R.H. Cole, *J. Chem. Phys., 9* (1941) 341.
21 D.W. Davidson and R.H. Cole, *J. Chem. Phys., 19* (1951) 1484.
22 A.K. Jonscher, *Dielectric Relaxation in Solids,* Chelsea Dielectrics Press, London, 1983.
23 C.D. Jaeger, S.C. Levy, E.V. Thomas and J.T. Cutchen, *J. Power Sources, 20* (1987) 27.
24 C.D. Jaeger, N.H. Hall and E.V. Thomas, Lithium ambient-temperature battery reliability program, *SAND87-2119*, Sandia National Laboratories, Albuquerque, NM, USA, 1989.
25 C.D. Jaeger, Improved Li/SO_2 cell reliability using complex impedance analysis, *Proc. Symp. Lithium Batteries, 1987,* Vol. 87-1, The Electrochemical Society, Princeton, NJ, USA, Abstr. No. 93.
26 P.R. Roberge, M. Farahani and K. Tomantschger, *J. Power Sources, 41* (1993) 321.
27 A. Chabli, J.P. Diard, P. Landau and B. LeGorrec, *Electrochim. Acta, 29* (1984) 509.
28 C. Gabrielli, F. Huet and M. Keddam, in A. D'Amico and P. Mazetti (eds.), *Noise in Physical Systems and 1/f noise,* Elsevier, Amsterdam, 1986, p. 214.
29 G. Verville, P.R. Roberge and J. Smit, *Power Sources 12,* International Power Sources Symposium Committee, Leatherhead, UK, 1989, pp. 43–60.
30 G. Verville, P.R. Roberge, R. Beaudoin and J. Smit, *Proc. 9th Int. Electric Vehicle Symp., Toronto, Canada, Nov. 13–16, 1988,* EVSS88-060.
31 P.R. Roberge, R. Beaudoin, G. Verville and J. Smit, *J. Power Sources, 27* (1989) 177.
32 P.R. Roberge, E. Halliop and M.D. Farrington, *J. Power Sources, 34* (1991) 233.
33 P.C. Searson and J.L. Dawson, *J. Electrochem. Soc, 135* (1988) 1908.
34 K. Hladky and J.L. Dawson, *Corros. Sci., 22* (1982) 231.
35 J.C. Uruchurtu and J.L. Dawson, *Corrosion, 43* (1987) 19.
36 K. Tomantschger, R. Book, R. Findlay and E. Oran, Development of mercury-free reusable alkaline MnO_2–Zn consumer batteries, *Final Rep.* prepared for the Ontario Ministry of the Environment, BTI, 1992.
37 P.R. Roberge, *J Appl. Electrochem.,* in press.